Effect of interfacial mass transport on inertial spreading of liquid droplets

Cite as: Phys. Fluids **32**, 032101 (2020); https://doi.org/10.1063/1.5135728
Submitted: 07 November 2019 . Accepted: 13 February 2020 . Published Online: 02 March 2020

Lina Baroudi, and Taehun Lee

Physics of Fluids ARTICLE scitation.org/journal/phf

Effect of interfacial mass transport on inertial spreading of liquid droplets

Cite as: Phys. Fluids 32, 032101 (2020); doi: 10.1063/1.5135728
Submitted: 7 November 2019 • Accepted: 13 February 2020 •
Published Online: 2 March 2020

Lina Baroudi[1,a] and Taehun Lee[2,b]

AFFILIATIONS

[1] Department of Mechanical Engineering, Manhattan College, Riverdale, New York 10471, USA
[2] Department of Mechanical Engineering, City College of City University of New York, New York, New York 10031, USA

[a] Author to whom correspondence should be addressed: lina.baroudi@manhattan.edu
[b] Electronic mail: thlee@ccny.cuny.edu

ABSTRACT

In this work, the early time dynamics of low-viscosity liquid drops spreading in their saturated vapor on partially wetting surfaces are investigated by lattice Boltzmann numerical simulations. Attention is paid to the effect of vapor transport through condensation on the spreading process. We observe that the condensation current resulting from the slight supersaturation of the liquid vapor near the dynamic wetting meniscus contributes to the motion and affects the spreading dynamics. Our results indicate that, in order to properly capture the initial dynamics of inertial spreading of a relatively volatile liquid drop, it is important to account for the vapor transport through condensation in the immediate vicinity of the contact line. A direct qualitative and quantitative comparison with experimental data of spontaneously wetting liquid drops is presented.

I. INTRODUCTION

When a liquid drop makes contact with a solid surface, the contact line moves until the liquid/solid/vapor system reaches the equilibrium state. This process is known as spreading and corresponds to the contact line between the vapor, liquid, and solid moving across the solid surface. The spreading dynamics of the liquid on solid surfaces is relevant to many natural and engineering processes ranging from pollutant oil wetting fish scales[1] and hydrophobic feet of insects[2] to inkjet printing,[3,4] coating,[5] and water–oil mixtures in oil recovery.[6] All these phenomena are governed by the surface and interfacial interactions acting at very small distances. Due to the ubiquity of the spreading process, it has attracted the attention of researchers for many years and still does.[7,8] General reviews of wetting phenomena are given by de Gennes,[9] Bonn *et al.*,[10] Snoeijer and Andreotti,[11] and Sui *et al.*[12] Despite the apparent simplicity of a spreading liquid drop on a solid surface, the evolution of the drop is difficult to investigate analytically as the classical continuum hydrodynamic description of the contact line motion under the usual no slip condition at the solid surface leads to a non-integrable stress singularity.[9,13,14] Various mechanisms have been proposed to resolve this non-physical divergence. One common approach in numerical solutions of the Navier–Stokes equations is to introduce a boundary condition with a stress- or velocity-dependent slip at the solid surface in the vicinity of the three-phase point.[15,16] The other extreme approach to describe the contact line motion is to directly resolve all regions of the flow, such as in molecular dynamics (MD) simulations. MD simulations give useful information on the effects of diffuse boundary and effective slip at molecular distances.[17,18] Such simulations, however, require a prohibitively large computational effort and, thus, are restricted to small systems and simple model fluids. Even hybrid approaches in which MD simulation around a contact line is coupled to a continuum model still suffer from the same problem.[10]

A middle ground is taken by mesoscale modeling techniques, which offer alternative explanations of contact line motion without relying on the breakdown of the no slip condition. These approaches incorporate a diffuse interface,[19–30] thus removing any contact line singularity. They are also able to address longer length- and time-scales than molecular dynamics. Seppecher[19] established the governing equations for isothermal flow in the Stokes regime near a moving contact line on a planar solid wall using a diffuse interface model. He showed that the curvature of the interface in the vicinity of the contact line drives mass transport through the interphase

boundary, which served as an effective slip mechanism relieving the viscous stress singularity. Pismen and Pomeau[23] applied the phase field model to study spreading of thin liquid films in the lubrication limit and also observed that phase change may strongly affect the dynamics near the contact line. Briant *et al.*[25] studied the steady-state interface profile of a droplet held between two shearing walls by the lattice Boltzmann approach and showed that the contact line singularity is overcome by evaporation or condensation near the contact line, which is driven by the curvature of the diffuse interface.

All the above-mentioned diffuse interface numerical studies of contact line motion[19,23,25] in different flow geometries have reported that the curvature of the interface near the contact line leads to mass transport across the interface. However, these studies were restricted to the steady state, lubrication limit, or Stokes flow regime, and none of the reported results were directly compared to the experimental data. The focus of this work is on determining the influence of mass transfer across the interface through condensation on the early time dynamics of inertial spreading and comparing the numerical results reported in this work to the experimental results obtained by Bird *et al.*[31] As all liquids are volatile to a certain extent, it is expected that phase change can aid the contact line motion with the no slip boundary condition applied at the solid boundary. It actually seems natural to expect that phase change can aid contact line motion.[32,33] Evaporation/condensation has first been proposed by Hardy[34] as a possible mechanism for controlling the contact line motion at the molecular scale. Derjaguin's concept of disjoining pressure has been used by Wayner and co-workers in order to investigate this possibility.[35–39] Recently, a theory for liquid transport by evaporation and re-condensation has been suggested, in which use is made of Kelvin's equation, giving the dependence of the equilibrium vapor pressure of a liquid on the curvature of its exposed surface.[32,40–42]

Although the later stages of the spreading phenomena close to equilibrium are well understood from the work of Voinov,[43] Cox,[44] and Tanner,[45] the physical mechanisms governing the initial spreading dynamics right after a liquid drop make contact with a partially wetting solid surface is not yet fully understood, especially when phase change is involved. The spreading behavior without phase change effects is characterized by the Ohnesorge number $Oh = \eta_l/(\rho_l \sigma R_0)^{1/2}$ and the fluid–solid interactions represented by equilibrium contact angle θ_{eq}, where η_l is the liquid viscosity, ρ_l is the liquid density, σ is the liquid–vapor surface tension, and R_0 is the initial drop radius. Considering the type of force resisting the spreading drop deformation and in the absence of gravitational forces, the spreading process has been classified either as a two-regime process for low-viscosity liquids ($Oh < 1$), where the spreading process starts in an inertia dominated regime[31,46–48] followed by a viscosity dominated regime close to equilibrium,[43–45] or as a single viscosity dominated process for high-viscosity liquids ($Oh > 1$).[49,50]

For low-viscosity liquids, the initial stages of spreading on a completely wetting surface are strongly reminiscent of the inertial coalescence of two freely suspended spherical liquid drops.[46,51–53] In both systems, the spreading radius r follows a power law scaling with a spreading exponent $\alpha = 0.5$.[46] However, for drops spreading on partially wetting surfaces, the initial spreading dynamics were found to depend strongly on surface wettability, $r \sim t^{\alpha}$, with a non-universal exponent α that varies systematically with the equilibrium contact angle.[31,54,55] In the final stage of inertial spreading, close to equilibrium, the drop spreads following Tanner's law, which relates the contact radius with time as $r \sim t^{1/10}$.[45]

In this study, we investigate the effect of condensation transport on the early time dynamics of inertial spreading of a liquid drop within the framework of lattice Boltzmann simulations. To explore how condensation affects the early time dynamics of inertial spreading, we utilize two lattice Boltzmann equation (LBE) approaches to model the spreading of a liquid drop in contact with an atmosphere of its pure vapor. The first is a non-ideal fluid LBE model,[56] which is employed to model the condensation-assisted spreading (CAS). The second is a two phase fluid (nearly) incompressible LBE model,[57] and it is employed to model the spreading of a liquid drop without condensation effects. The comparison between the results of the two methods establishes the sensitivity of the results to condensation as an additional mechanism that influences the spreading dynamics at early times. The methods are briefly discussed in Sec. II, before the presentation of the results in Sec. III. The numerical results are compared to the previous experimental results of spontaneously wetting liquid drops in the inertial regime.[31]

II. NUMERICAL METHODS

The discrete Boltzmann equation (DBE) for mass and momentum of nonideal fluids with external force can be written as

$$D_t f_\alpha = \partial_t f_\alpha + e_{\alpha i}\partial_i f_\alpha = -\frac{f_\alpha - f_\alpha^{eq}}{\lambda} + \frac{(e_{\alpha i} - u_i)F_i}{\rho c_s^2} f_\alpha^{eq}, \tag{1}$$

where f_α is the particle distribution function along the α direction, $e_{\alpha i}$ is the i component of the α-direction microscopic velocity, u_i is the macroscopic velocity, ρ is the density, $c_s^2 = (\partial_\rho p)_s$ is the square of speed of sound at constant entropy (s), λ is the relaxation time, F_i models the intermolecular attraction and the effects of the exclusion volume of the molecules on the equilibrium properties of a dense gas, and p is the pressure. The equilibrium distribution function f_α^{eq} is given by

$$f_\alpha^{eq} = t_\alpha \rho \left[1 + \frac{e_{\alpha i}u_i}{c_s^2} + \frac{(e_{\alpha i}e_{\alpha j} - c_s^2\delta_{ij})u_i u_j}{2c_s^4}\right], \tag{2}$$

where t_α is a weighting factor.[58] In the case of a pseudo-van der Waals fluid without the effect of gravity, the intermolecular attraction expressed in the potential form to avoid the development of the parasitic currents[56] can be written as

$$F_i = \partial_j \rho c_s^2 \delta_{ij} - \rho\partial_i(\mu_0 - \kappa\partial_j^2\rho), \tag{3}$$

where μ_0 is the bulk chemical potential and κ is the gradient parameter related to the magnitude of the surface tension force. The equilibrium properties of a system without wall boundary can be described by a bulk free energy $\psi_b = \int_\Omega \left(E_0(\rho) + \frac{\kappa}{2}\partial_k\rho\partial_k\rho\right)d\Omega$. In the pseudo-van der Waals fluid, E_0 can be approximated as $E_0(\rho) \approx \beta(\rho - \rho_v^{sat})^2(\rho - \rho_l^{sat})^2$,[59] where β is a constant that is related to the compressibility of bulk phases and ρ_v^{sat} and ρ_l^{sat} are the densities of vapor and liquid phases at saturation, respectively. Given the thickness of the diffuse interface ϵ, the gradient parameter and the liquid–vapor

surface tension σ could be calculated as $\kappa = \beta\epsilon^2\left(\rho_l^{sat} - \rho_v^{sat}\right)^2/8$ and $\sigma = \left(\rho_l^{sat} - \rho_v^{sat}\right)^3/6\sqrt{2\kappa\beta}$, respectively. In Eq. (3), the bulk chemical potential is related to E_0 by $\mu_0 = \partial_\rho E_0$ and to the pressure p by the equation of state $p = \rho\partial_\rho E_0 - E_0$, which leads to $\partial_i p = \rho\partial_i\mu_0$. Considering short-ranged fluid–solid interactions such that they contribute a surface integral to the total free energy of the system, the boundary condition for the Laplacian of density in Eq. (3) can be established by considering the following additional wall free energy $\psi_s = -\phi_1\rho_s$, where ϕ_1 is a constant describing the wetting properties in the regime of partial wetting and ρ_s is the density at the solid surface. Then, the total free energy takes the following form: $\psi_b + \psi_s = \int_\Omega\left(E_0(\rho) + \frac{\kappa}{2}\partial_k\rho\partial_k\rho\right)d\Omega - \int_\Gamma(\phi_1\rho_s)d\Gamma$. This imposes the boundary condition for $\partial_j^2\rho$ in Eq. (3) as $\kappa\partial_n\rho_s = -\phi_1$. At the solid surface, the equilibrium boundary condition[60,61] is imposed for the calculation of the unknown particle distribution function and the bounce-back rule guaranteeing the mass and momentum conservation is invoked as well.

The DBE [Eq. (1)] for the mass and momentum equations is transformed into that for the isothermal pressure evolution and momentum equations. The details of this transformation are shown in the Appendix. The validations and implementation of the two LBE models are described in Refs. 56, 57, 60, and 62. The macroscopic equations recovered from the two LBE models through the Chapman–Enskog expansion are the continuity, momentum, and isothermal pressure evolution equations described as follows:

$$\partial_t\rho + \partial_i(\rho u_i) = 0, \tag{4}$$

$$\partial_t(\rho u_i) + \partial_j(\rho u_i u_j) = -\partial_j p\delta_{ij} + \partial_j\sigma_{ij}^{(v)} + \kappa\rho\partial_i(\partial_j^2\rho), \tag{5}$$

$$\partial_t p + \rho(\partial_\rho p)\partial_i u_i + u_i\partial_i p = 0. \tag{6}$$

Here, $\sigma_{ij}^{(v)}$ is the viscous stress tensor. In essence, the two LBE models differ only by the way the pressure is updated. In the non-ideal fluid LBE model, $\partial_\rho p$ for a typical cubic equation of state (EOS) is not constant and turns negative at the phase interfaces, which may trigger isothermal phase change due to pressure variation.[62] In the incompressible LBE model, $\partial_\rho p$ is assumed to be constant and positive, and consequently, phase change is not allowed to take place.

III. RESULTS AND DISCUSSION

A. Simulation setup

In our numerical simulations, spreading of a two-dimensional (2D) liquid drop of radius $R_0 = 400$ lattice units (*l.u.*) in contact with an atmosphere of its pure vapor, generated on a 4000 × 2000 l.u. computational domain, is studied. The boundaries are all symmetric except at the solid surface, where the wall boundary condition presented in Sec. II is imposed. Contact problems such as coalescence and spreading are known to be essentially 2D phenomena,[47,51,63] and the same is expected here. It has been shown[51] that ω, the height of the meniscus [Fig. 1(a)], gives the driving curvature as it is always smaller than the contact radius r (Fig. 1). Thus, at initial times, the three-dimensional problem has similar asymptotic behavior as the two-dimensional one.

The surface tension, density, and bulk viscosity of the simulated fluid are fixed with $Oh = 0.1$. The liquid/vapor density and viscosity ratios, the interfacial thickness, and the parameter β are $\rho_l/\rho_v = 10$, $\mu_l/\mu_v = 10$, $\epsilon = 4$ *l.u.*, and $\beta = 0.02$, respectively. The nondimensional measure for the interface thickness is the Cahn number, defined by $Cn = \epsilon/2R_0$, and has a value of $4/800 = 0.005$ in the simulations. The parameter β, ϵ, and Cn are fixed in all the simulations, unless otherwise mentioned. The Bond number defined as $Bo = (\rho_l - \rho_v)gR_0^2/\sigma$, with g being the gravity, is set to zero in all simulations. Grid resolution analysis is performed using a grid size as a function of the initial radius of the drop $10R_0 \times 5R_0$ with the equilibrium contact angle $\theta_{eq} = 30^\circ$ while keeping the interfacial thickness fixed $\epsilon = 4$ *l.u.* The sizes of the grids used in this analysis are 4000 × 2000, 6000 × 3000, and 8000 × 4000. Figure 2 presents the effect of gird refinement on the time evolution of the spreading contact radius resulting from the non-ideal fluid LBE model [condensation-assisted spreading (CAS)] and the two phase fluid (nearly) incompressible LBE model (spreading without condensation effects). The contact radius is scaled by the initial drop radius R_0 and time by the inertial time scale $t_i = \sqrt{\rho_l R_0^3/\sigma}$. We observe in Fig. 2 that grid refinement does not have significant impact on the results. Thus, for the droplet radius $R_0 = 400$ *l.u.* used in our simulations, the results are essentially independent of increased grid resolution. A domain size dependency test is performed using different domain sizes. For the domain of size 4000 × 2000 *l.u.*, the increased size of the domain has negligible influence on the spreading process.

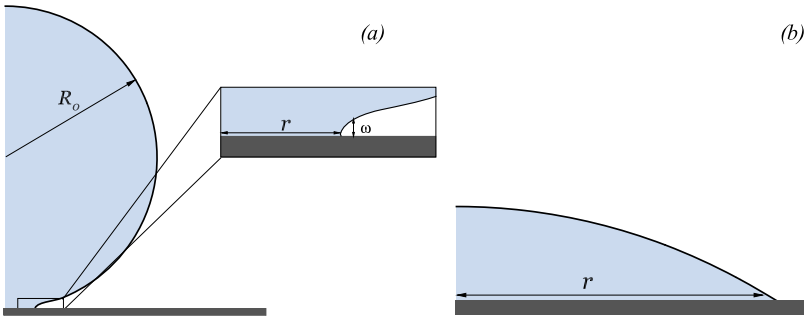

FIG. 1. (a) Schematics showing the geometry of the drop during the initial stages of spreading. R_0 is the initial drop radius, and r is the contact radius. The height of the meniscus ω determines the local curvature and, thus, the driving force. (b) Schematics showing the geometry of the drop during the late stages of spreading.

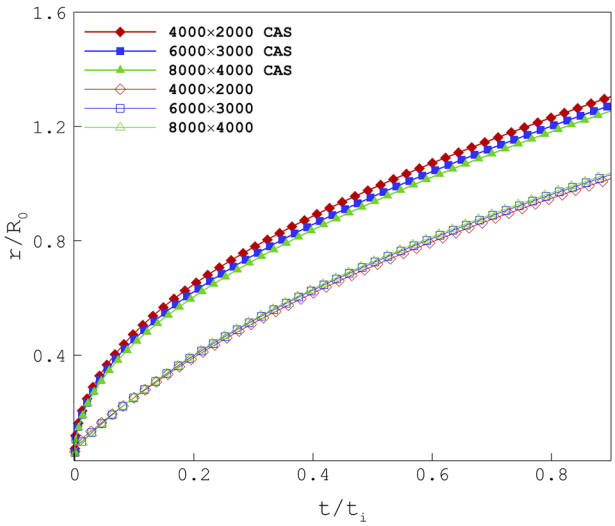

FIG. 2. Effect of grid resolution on the temporal evolution of the contact radius. Filled symbols correspond to condensation-assisted spreading (CAS) resulting from the non-ideal fluid LBE, and open symbols correspond to spreading without condensation effects resulting from the two phase fluid incompressible LBE.

B. Flow field and interfacial profiles

Figure 3 compares the velocity field in the vicinity of the contact line [the inset in Fig. 1(a)] from the simulation results of the spreading without condensation effects [Figs. 3(a) and 3(c)] with that of the condensation-assisted spreading [Figs. 3(b) and 3(d)] at t/t_i = 0.2 [Figs. 3(a) and 3(b)] and t/t_i = 0.4 [Figs. 3(c) and 3(d)] with an equilibrium contact angle of $\theta_{eq} = 3°$, where t_i is inertial time scale defined above. The liquid–vapor interface is represented by an iso-density level $(\rho_l^{sat} + \rho_v^{sat})/2$. As the liquid drop contacts the solid surface, the interface becomes highly curved close to the contact point, with a meniscus characterized by a small height as shown in Fig. 1(a). This strongly curved meniscus generates a rapid flow toward the contact line region due to the gradient in Laplace pressure between the drop's periphery and its center. As the drop spreads without condensation effects [Figs. 3(a) and 3(c)], we observe that vapor escapes radially away from the moving contact line. However, the velocity field resulting from the condensation-assisted spreading [Figs. 3(b) and 3(d)] shows a different trend. In Figs. 3(b) and 3(d), the velocity vectors in the vapor phase are directed toward the contact line indicating mass transfer across iso-density lines of the interface, which represents condensation of the vapor phase at the interface. The condensation in our simulations is signaled by the negative divergence of the velocity field $\partial_i u_i < 0$. The highly curved contact meniscus leads to an effective slight supersaturation of the liquid vapor. If the spreading liquid is volatile to some extent, then local condensation ensues. The coupling between the liquid meniscus curvature and the mass exchange across the interface is provided by the Kelvin effect. Directly over the curved interface of a liquid meniscus, the local vapor pressure of the liquid is determined by the curvature, as described by the classic Kelvin equation $p_v = p_v^{sat} \exp[\frac{-\sigma v_l}{RT\omega_{eq}}]$, where p_v is the vapor pressure, p_v^{sat} is the saturation vapor pressure, ω_{eq} is the equilibrium radius of curvature of the meniscus (Kelvin radius), and v_l, R, and T are liquid molar volume, ideal gas constant, and temperature, respectively. This equation has to be modified in the presence of a solid surface, and solid–fluid interactions must be taken into account. However, the modified Kelvin equation retains the prediction that a concave meniscus requires a lower local vapor

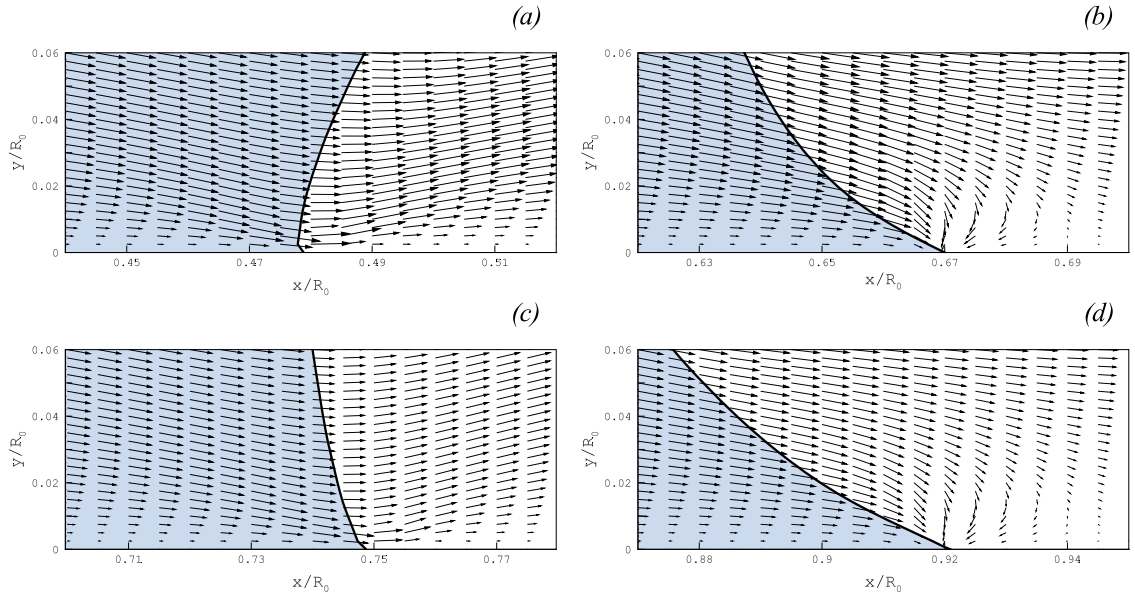

FIG. 3. The velocity field in the contact line region at t/t_i = 0.2 [(a) and (b)] and t/t_i = 0.4 [(c) and (d)], resulting from the spreading without condensation effects [(a) and (c)] and the condensation-assisted spreading [(b) and (d)]. The velocity vectors in [(a) and (b)] and [(c) and (d)] are plotted with the same scale.

pressure to stay at equilibrium than a planar surface. An advancing liquid interface presents greater concavity than when at equilibrium. As a consequence, vapor coming from elsewhere on the macroscopic part of the drop (of greater convexity) may re-condense near the contact line.[41,42]

Assuming short-ranged solid–fluid interactions compared to the thickness of the diffuse vapor–liquid interface, an additional wall free energy contribution to the overall energy is considered. For the wall free energy functional ψ_s utilized in our models, the modified Kelvin equation is then written as $p_v = p_v^{sat}\exp[\frac{v_l}{RT}(\frac{-\sigma}{\omega_{eq}} - \Pi(h))]$, where $\Pi(h)$ is the disjoining pressure between the vapor–liquid and liquid–solid interfaces and h denotes the dynamic interfacial profile height from the solid surface. The disjoining pressure represents the shift of chemical potential in the proximity of the solid surface and is dependent on the boundary conditions at the solid surface. For exponentially decaying solid–fluid interactions, Π is computed in the framework of the phase field theory[23] and is given by $\Pi = \frac{-2\kappa}{\phi_1}\exp(-h/\epsilon)(1 - \frac{1}{\phi_1}\exp(-h/\epsilon))$. For large h, the disjoining pressure becomes negligible, and at small h, it is not singular as in the sharp-interface theories with van der Waals interactions. In the modified Kelvin equation, the saturation vapor pressure, surface tension, and molar volume are all properties of the fluid at equilibrium and are considered constants with respect to the system. Temperature is also considered constant in the Kelvin equation as it is a function of the saturation vapor pressure. The condensation of vapor results in the release of latent heat and increases the temperature difference between the condensed liquid and the surrounding vapor phase. It is unlikely that the heat released by the condensation of vapor could give rise to a large value of ΔT.[64] Here, we assume large thermal conductivity and isothermal phase change.[59]

From the modified Kelvin equation, we may calculate the appropriate equilibrium pressure of vapor, p_v, where the drop profile is at equilibrium with this geometry. Excess vapor pressure, Δp, driving local condensation from the ambient saturated vapor is then given by $\Delta p_v = p_v^{sat} - p_v = p_v^{sat}\{(1 - \exp[\frac{v_l}{RT}(\frac{-\sigma}{\omega_{eq}} - \Pi(h))])\}$, where the net rate of condensation J_c is proportional to the vapor excess pressure $J_c \sim \Delta p$.[41,65] The condensation current resulting from the modified curvature of the dynamic wetting meniscus near the contact line contributes to the motion and affects the spreading rate. This effect is expected to be important in a small region of the liquid meniscus very close to the contact line,[66] where phase change self-adjusts to the contact line motion according to the modified Kelvin equation. Figure 4 shows the divergence of the velocity field $\partial_i u_i$ at an early time $t/t_i = 0.2$ [Fig. 4(a)] and at a later time $t/t_i = 1.2$ [Fig. 4(b)] in the spreading process. The darker color represents the more negative value of $\partial_i u_i$, i.e., higher condensation rate. As shown in Fig. 4, the intensity of the divergence field is reduced with time as the condensation rate self-adjusts to the contact line motion.

Figure 5 shows snapshots of the droplet as it wets different solid surfaces with an equilibrium contact angle of $\theta_{eq} = [3°, 60°, 120°]$. The right half of each panel in Fig. 5 shows the results of the condensation-assisted spreading, and the left half shows the results of spreading without condensation effects. Each panel has six snapshots in time of the droplet as it spreads across the solid surface. The first snapshot is at time 1 ($t/t_i = 0.04$), and the droplet spreads across the surface in the successive times 2, 3, 4, 5, and 6. The droplet initially forms a large contact angle when it starts to wet the surface. As it spreads on the surface, the dynamic contact angle relaxes toward its equilibrium value θ_{eq}. In the initial times of the spreading, the dynamic contact angle varies rapidly. We note that the results of

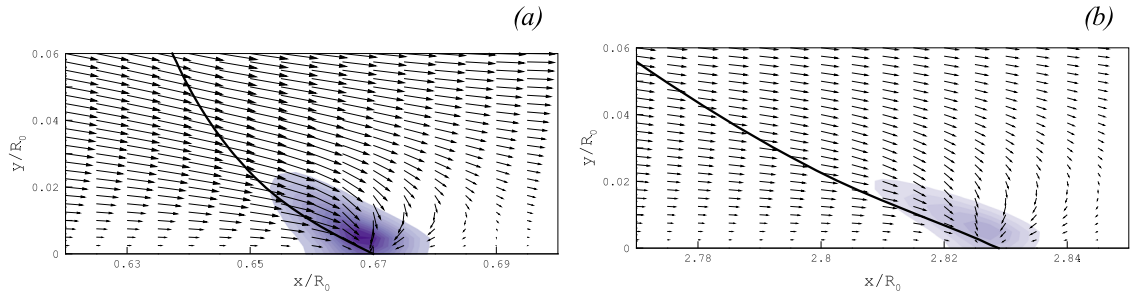

FIG. 4. The color field represents the divergence of the velocity field $\partial_i u_i$ at $t/t_i = 0.2$ (a) and at $t/t_i = 1.2$ (b). The velocity vectors in (a) and (b) are plotted with the same scale.

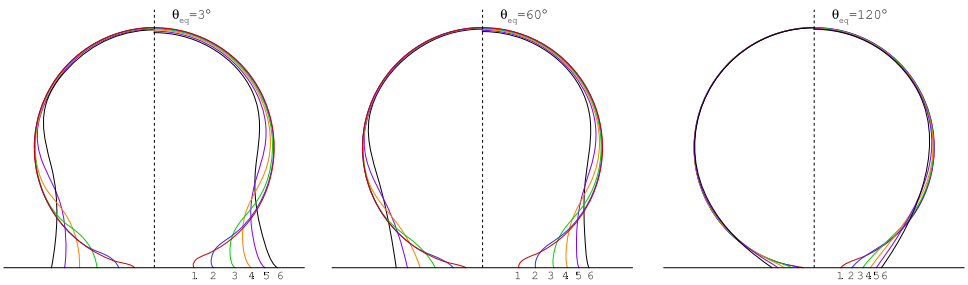

FIG. 5. Droplet shapes at (1) $t/t_i = 0.04$, (2) $t/t_i = 0.1$, (3) $t/t_i = 0.2$, (4) $t/t_i = 0.3$, (5) $t/t_i = 0.4$, and (6) $t/t_i = 0.5$ for three different surfaces: $\theta_{eq} = [3°, 60°, 120°]$. The right half of each panel shows the condensation-assisted spreading, and the left half shows the spreading of the droplet without condensation effects.

the condensation-assisted spreading (right half) show faster relaxation toward the equilibrium contact angle and lower curvature in the vicinity of the contact line compared to spreading without condensation effects (left half). The two LBE models predict a somewhat different shape of the droplet interface. We see clearly that the contact line in the case of condensation-assisted spreading propagates faster than spreading without condensation effects. Condensation modifies the liquid profile and, therefore, the flow field. There is a mutual interdependence between the dynamic contact angle and the local flow field. Thus, condensation current causes a change in the apparent dynamic contact angle and results in a faster relaxation toward the equilibrium contact angle compared to the spreading without condensation effects.

C. Temporal contact line evolution

The temporal evolution of the contact radius during the initial stages of wetting as the droplet spreads on five different surfaces [θ_{eq} = 4°, θ_{eq} = 30°, θ_{eq} = 60°, θ_{eq} = 90°, and θ_{eq} = 120°] with and without condensation effects is presented and compared to the experimental results by Bird *et al.*[31] in Fig. 6. The contact radius is scaled by the initial drop radius R_0, and time is scaled by the inertial time scale t_i. The experiments by Bird *et al.*[31] provided detailed analysis of first steps of spreading of inviscid liquid (water and water–glycerol mixtures) droplets over solid surfaces with different degrees of wettability. The results presented in Fig. 6 show that a faster time evolution of the spreading radius is observed for condensation-assisted spreading on all surfaces compared to spreading without condensation effects. As discussed in Sec. III B, the condensation current resulting from the modified curvature of the dynamic wetting meniscus contributes to the motion and results in a faster spreading rate. In the case of condensation-assisted spreading, the motion of the contact line involves both a hydrodynamic current resulting from the gradient in Laplace pressure, J_h, and a condensation current, J_c, and the total speed of the contact line has both hydrodynamic and condensation contributions.[42] When the condensation effects are considered negligible, the contact line speed has only hydrodynamic contribution, which results in a slower evolution of the contact line compared to the evolution of the condensation-assisted spreading.

The results of the condensation-assisted spreading show good agreement with the experimental results by Bird *et al.*[31] on three surfaces with equilibrium contact angles [θ_{eq} = 3°, 43°, and 117°] (Fig. 6). Excellent agreement is observed for the spreading on hydrophilic and hydrophobic surfaces. Our results indicate that in order to correctly capture the wetting speed and recreate the wetting physics observed experimentally, it is crucial to account for condensation effects in the vicinity of the contact line region when modeling the spreading of relatively volatile liquids. Neglecting condensation effects results in a slower spreading rate compared to the experimental data reported by Bird *et al.*[31] Shanahan[42] investigated the effect of condensation transport on the spreading of water using a model he proposed and observed that condensation currents result in a higher spreading rate in agreement with the results presented here.

In Fig. 7, the evolution of the contact radius is plotted vs time in logarithmic units along with the experimental data for a longer range of time. It is clear from Fig. 7 that the spreading radius follows a power law $\frac{r}{R_0} = C(\frac{t}{t_i})^{\alpha}$, whose exponent α depends on the wetting properties of the solid surface, where the drop with lower θ_{eq} spreads faster than the drop with higher θ_{eq}.[31,55] We also observe a distinct change in the exponent of the simulation results for spreading with and without condensation effects and the experimental data when dimensionless time has a value around 2. This shift in the exponent corresponds to cross over from inertial to viscous spreading.

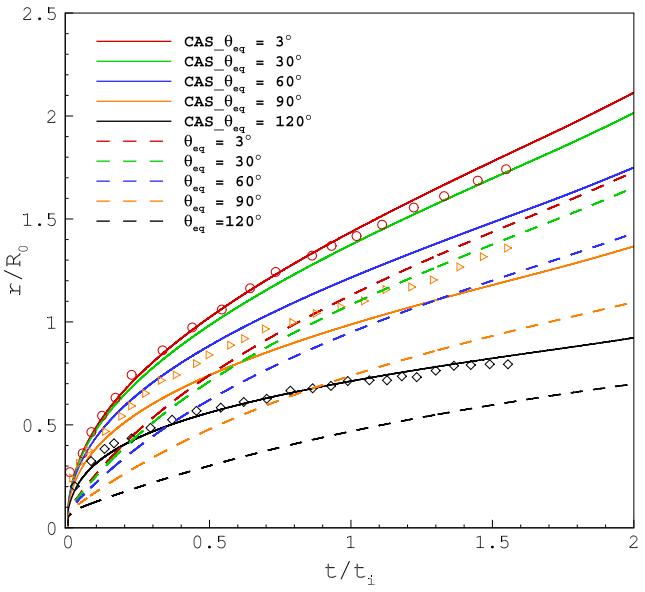

FIG. 6. Temporal contact line evolution for θ_{eq} = 3°, θ_{eq} = 30°, θ_{eq} = 60°, θ_{eq} = 90°, and θ_{eq} = 120°. Full lines correspond to condensation-assisted spreading (CAS), and dashed lines correspond to spreading without condensation effects. The experimental results of Ref. 31 are given by open circles, triangles, and diamond shaped markers for θ_{eq} = 3°, θ_{eq} = 43°, and θ_{eq} = 117°, respectively.

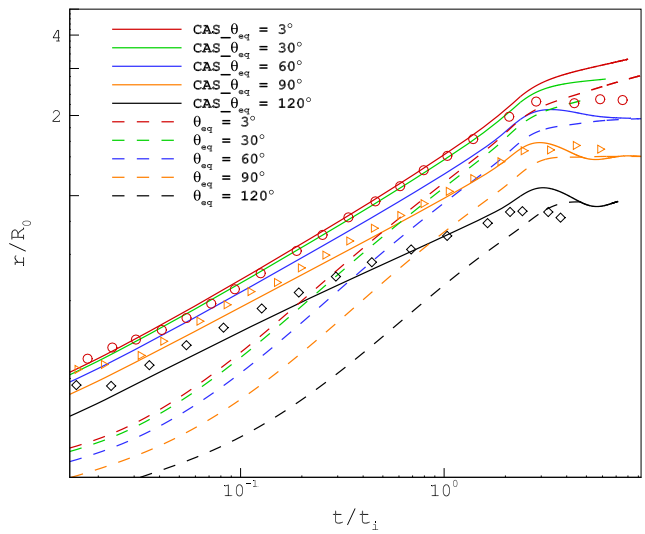

FIG. 7. A log–log plot of the data presented in Fig. 6 for a longer time range.

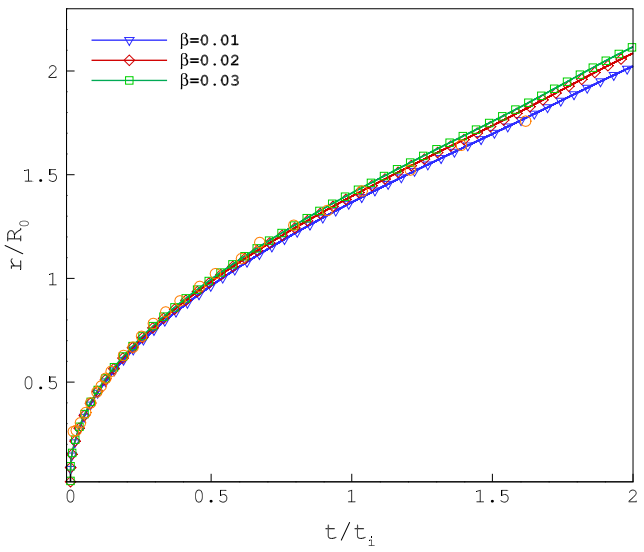

FIG. 8. Effect of β on the time evolution of the condensation-assisted spreading contact radius for θ_{eq} = 3° and Oh = 0.1. The experimental results[31] for θ_{eq} = 3° are given by open circle markers.

Biance *et al.*[46] provided an estimate for the duration of the inertial regime and calculated the characteristic time required for the crossover from the inertial to the viscous regime as $\tau_c \sim (\frac{\rho_l \sigma R_0}{\eta_l^2})^{1/8} t_i$. By introducing the parameters used in the simulated cases, we obtain $\tau_c/t_i \approx 1.8$, which is in good agreement with the experimental and numerical data presented in Fig. 7. The slight discrepancy between the experimental data and the numerical results of the condensation-assisted spreading at late times is an effect of differences in the experimental and computational setup. At late times in the experiments, the droplet starts to detach from the needle. In the simulations, the liquid drop is freely suspended and not attached to a rod. It is noteworthy that the effect of condensation on the spreading behavior becomes less important at later times close to equilibrium, and the difference between the curves corresponding to spreading with and without condensation effects for all θ_{eq} becomes very small.

Finally, we discuss the effect of the parameter β on the spreading rate. The parameter β in the LBE models is related to the speed of sound, and thus, changing β implies the modification of the speed of sound. The effect of β on the condensation-assisted spreading is plotted in Fig. 8 for β = 0.03, 0.02, and 0.01, θ_{eq} = 3°, and Oh = 0.1 along with the experimental results for θ_{eq} = 3°. We note that the higher β results in slightly faster evolution of the contact line. The differences in the results are minor in this range of β. After determining β, the model has, in principle, no adjustable parameters. The width of the interface ϵ is chosen to be the smallest numerically sustainable value above which the LBE method becomes unstable or the interface shape is distorted.

IV. CONCLUSIONS

We have numerically investigated the effect of condensation transport on the spontaneous spreading of low-viscosity liquid droplets on solid surfaces with different degrees of wettability. Two LBE models are utilized to capture the effect of condensation transport on the dynamics. We show that in order to correctly capture the dynamic wetting phenomena of relatively volatile spreading liquid droplets, the condensation effects have to be taken into account when modeling the spreading process. In the case of condensation-assisted spreading, the total spreading speed contains both hydrodynamic and condensation contributions, and thus, the spreading process initially proceeds faster in time. The condensation current modifies the liquid profile and, therefore, the flow field and the dynamic contact angle. The condensation flux self-adjusts to the contact line motion according to the modified Kelvin's equation, and its effect on the spreading becomes less important at late times close to equilibrium. In the case of condensation-assisted spreading, a good qualitative and quantitative agreement between the numerical and experimental[31] temporal evolution of the spreading radius is obtained. A good match is found for the time of transition from inertial to viscously dominated wetting between the simulations and the theory proposed by Biance *et al.*[46]

ACKNOWLEDGMENTS

T.L. acknowledges the support from the National Science Foundation under Award No. 1743794.

APPENDIX: DISCRETE BOLTZMANN EQUATION FOR PRESSURE AND MOMENTUM

The DBE [Eq. (1)] for the mass and momentum equations is transformed into that for the isothermal pressure evolution and momentum equations.[62,67] In order to perform the transformation, a new particle distribution function is defined as

$$g_\alpha = f_\alpha c_s^2 + (p - \rho c_s^2)\Gamma_\alpha(0), \tag{A1}$$

where $\Gamma_\alpha(\mathbf{u}) = f_\alpha^{eq}/\rho$. Taking the total derivative D_t of the new variable g_α gives

$$\begin{aligned} D_t g_\alpha &= c_s^2 D_t f_\alpha + D_t p \Gamma_\alpha(0) - c_s^2 D_t \rho \Gamma_\alpha(0) \\ &= -\frac{1}{\lambda}\left(g_\alpha - g_\alpha^{eq}\right) \\ &\quad + (e_{\alpha i} - u_i)\left[\partial_i \rho c_s^2 - \rho \partial_i(\mu_0 - \kappa \partial_j^2 \rho)\right]\Gamma_\alpha(\mathbf{u}) \\ &\quad + D_t p \Gamma_\alpha(0) - c_s^2 D_t \rho \Gamma_\alpha(0), \end{aligned} \tag{A2}$$

where the new equilibrium g_α^{eq} is

$$g_\alpha^{eq} = t_\alpha\left[p + \rho c_s^2\left(\frac{e_{\alpha i}u_i}{c_s^2} + \frac{(e_{\alpha i}e_{\alpha j} - c_s^2\delta_{ij})u_i u_j}{2c_s^4}\right)\right]. \tag{A3}$$

In the non-ideal fluid LBE model, the last two terms on the right-hand side of Eq. (A2) are expanded through the continuity equation as follows:

$$D_t p = \partial_t p + e_{\alpha i}\partial_i p = -\partial_\rho p \partial_i \rho u_i + e_{\alpha i}\partial_i p \tag{A4}$$

and

$$D_t \rho = \partial_t \rho + e_{\alpha i}\partial_i \rho = -\partial_i \rho u_i + e_{\alpha i}\partial_i \rho. \tag{A5}$$

In the incompressible LBE model, the divergence free condition, i.e., $\partial_i u_i = 0$, is applied to the above two equations and Eqs. (A4) and (A5) reduce to

$$D_t p = -\partial_\rho p \partial_i \rho u_i + e_{\alpha i}\partial_i p = (e_{\alpha i} - u_i)\partial_i p \tag{A6}$$

and

$$D_t \rho = -\partial_i \rho u_i + e_{\alpha i}\partial_i \rho = (e_{\alpha i} - u_i)\partial_i \rho. \tag{A7}$$

Now that the DBE for mass and momentum has been transformed into the DBE for pressure and momentum, and another set of distribution function for density is needed. For this purpose, Eq. (1) suffices.

REFERENCES

[1] P. R. Waghmare, N. S. K. Gunda, and S. K. Mitra, "Under-water superoleophobicity of fish scales," Sci. Rep. **4**, 7454 (2014).
[2] M. J. Hancock, K. Sekeroglu, and M. C. Demirel, "Bioinspired directional surfaces for adhesion, wetting, and transport," Adv. Funct. Mater. **22**, 2223 (2012).
[3] J. Z. Wang, Z. H. Zheng, H. W. Li, W. T. S. Huck, and H. Sirringhaus, "Dewetting of conducting polymer inkjet droplets on patterned surfaces," Nat. Mater. **3**, 171 (2004).
[4] B.-J. de Gans, P. C. Duineveld, and U. S. Schubert, "Inkjet printing of polymers: State of the art and future developments," Adv. Mater. **16**, 203 (2004).
[5] S. J. Weinstein and K. J. Ruschak, "Coating flows," Annu. Rev. Fluid Mech. **36**, 29 (2004).
[6] D. Saini and D. N. Rao, "Line tension-based modification of Young's equation for rock-oil-brine systems," SPE Reservoir Eval. Eng. **12**, 702 (2009).
[7] X. Liu, X. Zhang, and J. Min, "Spreading of droplets impacting different wettable surfaces at a Weber number close to zero," Chem. Eng. Sci. **207**, 495 (2019).
[8] F. C. Yang, X. P. Chen, and P. Yue, "Surface roughness effects on contact line motion with small capillary number," Phys. Fluids **30**, 012106 (2018).
[9] P. G. de Gennes, "Wetting: Statics and dynamics," Rev. Mod. Phys. **57**, 827 (1985).
[10] D. Bonn, J. Eggers, J. Indekeu, J. Meunier, and E. Rolley, "Wetting and spreading," Rev. Mod. Phys. **81**, 739 (2009).
[11] J. H. Snoeijer and B. Andreotti, "Moving contact: Lines scales, regimes, and dynamical transitions," Annu. Rev. Fluid Mech. **45**, 269 (2013).
[12] Y. Sui, H. Ding, and P. D. M. Spelt, "Numerical simulations of flows with moving contact lines," Annu. Rev. Fluid Mech. **46**, 119 (2014).
[13] C. Huh and L. E. Scriven, "Hydrodynamic model of steady movement of a solid/liquid/fluid contact line," J. Colloid Interface Sci. **35**, 85 (1971).
[14] E. B. Dussan, "On the spreading of liquids on solid surfaces: Static and dynamic contact lines," Annu. Rev. Fluid Mech. **11**, 371 (1979).
[15] E. B. Dussan, "The moving contact line: The slip boundary condition," J. Fluid Mech. **77**, 665 (1976).
[16] L. M. Hocking, "A moving fluid interface on a rough surface," J. Fluid Mech. **76**, 801 (1976).
[17] J. Koplik, J. R. Banavar, and J. F. Willemsen, "Molecular dynamics of fluid flow at solid surfaces," Phys. Fluids A **1**, 781 (1989).
[18] P. A. Thompson and M. O. Robbins, "Simulations of contact-line motion: Slip and the dynamic contact angle," Phys. Rev. Lett. **63**, 766 (1989).
[19] P. Seppecher, "Moving contact lines in the Cahn–Hilliard theory," Int. J. Eng. Sci. **34**, 977 (1996).
[20] D. Jacqmin, "Contact-line dynamics of a diffuse fluid interface," J. Fluid Mech. **402**, 57 (2000).
[21] H.-Y. Chen, D. Jasnow, and J. Viñals, "Interface and contact line motion in a two-phase fluid under shear flow," Phys. Rev. Lett. **85**, 1686 (2000).
[22] Y. Pomeau, "Contact line moving on a solid," Eur. Phys. J.: Spec. Top. **197**, 15 (2011).
[23] L. M. Pismen and Y. Pomeau, "Disjoining potential and spreading of thin layers in the diffuse interface model coupled to hydrodynamics," Phys. Rev. E **62**, 2480 (2000).
[24] L. M. Pismen, "Mesoscopic hydrodynamics of contact line motion," Colloids Surf., A **206**, 11 (2002).
[25] A. J. Briant, A. J. Wagner, and J. M. Yeomans, "Lattice Boltzmann simulations of contact line motion. I. Liquid-gas systems," Phys. Rev. E **69**, 031602 (2004).
[26] A. J. Briant and J. M. Yeomans, "Lattice Boltzmann simulations of contact line motion. II. Binary fluids," Phys. Rev. E **69**, 031603 (2004).
[27] X. D. Niu, Y. Li, Y. R. Ma, M. F. Chen, X. Li, and Q. Z. Li, "A mass-conserving multiphase lattice Boltzmann model for simulation of multiphase flows," Phys. Fluids **30**, 013302 (2018).
[28] M. Ebrahim, A. Ortega, N. Delbosc, M. C. T. Wilson, and J. L. Summers, "Simulation of the spreading of a gas-propelled micro-droplet upon impact on a dry surface using a lattice-Boltzmann approach," Phys. Fluids **29**, 072104 (2017).
[29] H. N. Dalgamoni and X. Yong, "Axisymmetric lattice Boltzmann simulation of droplet impact on solid surfaces," Phys. Rev. E **98**, 013102 (2018).
[30] W. Xiong and P. Cheng, "3D lattice Boltzmann simulation for a saturated liquid droplet at low Ohnesorge numbers impact and breakup on a solid surface surrounded by a saturated vapor," Comput. Fluids **168**, 130 (2018).
[31] J. C. Bird, S. Mandre, and H. A. Stone, "Short-time dynamics of partial wetting," Phys. Rev. Lett. **100**, 234501 (2008).
[32] A. Rednikov and P. Colinet, "Singularity-free description of moving contact lines for volatile liquids," Phys. Rev. E **87**, 010401 (2013).
[33] A. Rednikov and P. Colinet, "Contact-line singularities resolved exclusively by the Kelvin effect: Volatile liquids in air," J. Fluid Mech. **858**, 881 (2019).
[34] W. Hardy, "The spreading of fluids on glass," Philos. Mag. **38**, 49 (1919).
[35] P. C. Wayner, "The effect of interfacial mass transport on flow in thin liquid films," Colloids Surf. **52**, 71 (1991).
[36] P. C. Wayner, "Spreading of a liquid film with a finite contact angle by the evaporation/condensation process," Langmuir **9**, 294 (1993).
[37] M. Potash and P. C. Wayner, "Evaporation from a two-dimensional extended meniscus," Int. J. Heat Mass Transfer **15**, 1851 (1972).
[38] J. Schonberg and P. C. Wayner, "Spreading of a liquid film on a substrate by the evaporation—Adsorption process," J. Colloid Interface Sci. **152**, 507 (1992).
[39] P. C. Wayner, "Nucleation, growth and surface movement of a condensing sessile droplet," Colloids Surf., A **89**, 89 (1994).
[40] A. W. Adamson and A. P. Gast, *Physical Chemistry of Surfaces*, 6th ed. (Wiley, New York, 1997), p. 53.
[41] M. E. R. Shanahan, "Condensation transport in dynamic wetting," Langmuir **17**, 3997 (2001).
[42] M. E. R. Shanahan, "Spreading of water: Condensation effects," Langmuir **17**, 8229 (2001).
[43] O. V. Voinov, "Hydrodynamics of wetting," Fluid Dyn. **11**, 714 (1976).
[44] R. G. Cox, "The dynamics of the spreading of liquids on a solid surface. Part 1. Viscous flow," J. Fluid Mech. **168**, 169 (1986).
[45] L. H. Tanner, "The spreading of silicone oil drops on horizontal surfaces," J. Phys. D: Appl. Phys. **12**, 1473 (1979).
[46] A.-L. Biance, C. Clanet, and D. Quéré, "First steps in the spreading of a liquid droplet," Phys. Rev. E **69**, 016301 (2004).
[47] K. G. Winkels, J. H. Weijs, A. Eddi, and J. H. Snoeijer, "Initial spreading of low-viscosity drops on partially wetting surfaces," Phys. Rev. E **85**, 055301 (2012).
[48] A. Carlson, G. Bellani, and G. Amberg, "Universality in dynamic wetting dominated by contact-line friction," Phys. Rev. E **85**, 045302 (2012).
[49] A. Eddi, K. G. Winkels, and J. H. Snoeijer, "Short time dynamics of viscous drop spreading," Phys. Fluids **25**, 013102 (2013).
[50] S. Mitra and S. K. Mitra, "Understanding the early regime of drop spreading," Langmuir **32**, 8843 (2016).
[51] J. Eggers, J. R. Lister, and H. A. Stone, "Coalescence of liquid drops," J. Fluid Mech. **401**, 293 (1999).
[52] L. Duchemin, J. Eggers, and C. Josserand, "Inviscid coalescence of drops," J. Fluid Mech. **487**, 167 (2003).
[53] L. Baroudi, M. Kawaji, and T. Lee, "Effects of initial conditions on the simulation of inertial coalescence of two drops," Comput. Math. Appl. **67**, 282 (2014).

[54]L. Courbin, J. C. Bird, M. Reyssat, and H. A. Stone, "Dynamics of wetting: From inertial spreading to viscous imbibition," J. Phys.: Condens. Matter **21**, 464127 (2009).
[55]A. Carlson, M. Do-Quang, and G. Amberg, "Dissipation in rapid dynamic wetting" J. Fluid Mech. **682**, 213 (2011).
[56]T. Lee and P. F. Fischer, "Eliminating parasitic currents in the lattice Boltzmann equation method for nonideal gases," Phys. Rev. E **74**, 046709 (2006).
[57]T. Lee and C.-L. Lin, "A stable discretization of the lattice Boltzmann equation for simulation of incompressible two-phase flows at high density ratio," J. Comput. Phys. **206**, 16 (2005).
[58]Y.-H. Qian and S.-Y. Chen, "Dissipative and dispersive behavior of lattice-based models for hydrodynamics," Phys. Rev. E **61**, 2712 (2000).
[59]D. Jamet, O. Lebaigue, N. Coutris, and J. M. Delhaye, "The second gradient method for the direct numerical simulation of liquid-vapor flows with phase change," J. Comput. Phys. **169**, 624 (2001).
[60]T. Lee and L. Liu, "Wall boundary conditions in the lattice Boltzmann equation method for nonideal gases," Phys. Rev. E **78**, 017702 (2008).
[61]T. Lee and L. Liu, "Wall free energy based polynomial boundary conditions for non-ideal gas lattice Boltzmann equation," Int. J. Mod. Phys. C **20**, 1749 (2009).
[62]T. Lee and C.-L. Lin, "Pressure evolution lattice-Boltzmann-equation method for two-phase flow with phase change," Phys. Rev. E **67**, 056703 (2003).
[63]J. C. Burton and P. Taborek, "Role of dimensionality and axisymmetry in fluid pinch-off and coalescence," Phys. Rev. Lett. **98**, 224502 (2007).
[64]M. M. Kohonen, N. Maeda, and H. K. Christenson, "Kinetics of capillary condensation in a nanoscale pore," Phys. Rev. Lett. **82**, 4667 (1999).
[65]L. Baroudi, S. R. Nagel, J. F. Morris, and T. Lee, "Dynamics of viscous coalescing droplets in a saturated vapor phase," Phys. Fluids **27**, 121702 (2015).
[66]V. Janeček, F. Doumenc, B. Guerrier, and V. S. Nikolayev, "Can hydrodynamic contact line paradox be solved by evaporation–condensation?," J. Colloid Interface Sci. **460**, 329 (2015).
[67]X. Y. He, S. Chen, and R. Zhang, "A lattice Boltzmann scheme for incompressible multiphase flow and its application in simulation of Rayleigh–Taylor instability," J. Comput. Phys. **152**, 642 (1999).